TISSUE ENGINEERING

Photoactivated Composite Biomaterial for Soft Tissue Restoration in Rodents and in Humans

Alexander T. Hillel,[1]* Shimon Unterman,[2]* Zayna Nahas,[3] Branden Reid,[2] Jeannine M. Coburn,[4] Joyce Axelman,[2] Jemin J. Chae,[2] Qiongyu Guo,[2] Robert Trow,[5] Andrew Thomas,[5] Zhipeng Hou,[6] Serge Lichtsteiner,[7] Damon Sutton,[7] Christine Matheson,[7] Patricia Walker,[7] Nathaniel David,[7] Susumu Mori,[6] Janis M. Taube,[8] Jennifer H. Elisseeff[2]†

Soft tissue reconstruction often requires multiple surgical procedures that can result in scars and disfiguration. Facial soft tissue reconstruction represents a clinical challenge because even subtle deformities can severely affect an individual's social and psychological function. We therefore developed a biosynthetic soft tissue replacement composed of poly(ethylene glycol) (PEG) and hyaluronic acid (HA) that can be injected and photocrosslinked in situ with transdermal light exposure. Modulating the ratio of synthetic to biological polymer allowed us to tune implant elasticity and volume persistence. In a small-animal model, implanted photocrosslinked PEG-HA showed a dose-dependent relationship between increasing PEG concentration and enhanced implant volume persistence. In direct comparison with commercial HA injections, the PEG-HA implants maintained significantly greater average volumes and heights. Reversibility of the implant volume was achieved with hyaluronidase injection. Pilot clinical testing in human patients confirmed the feasibility of the transdermal photocrosslinking approach for implantation in abdomen soft tissue, although an inflammatory response was observed surrounding some of the materials.

INTRODUCTION

The body's soft tissue provides aesthetic form and physical structure, features that can be severely affected by trauma, disease, and aging, thus leading to deformities. Bony defects can be treated by autograft, allograft, or alloplastic implants; however, these options are not available for soft tissue defects, which often require multiple surgical procedures that can result in scars. Because facial soft tissue provides structural information related to identity of self, and because subtle deformities in this area severely affect social and psychological function, addressing these defects is of clinical importance (*1*). Native-tissue and materials-based (biological or synthetic) approaches have had limited success in replicating natural soft tissue structure over the long term, and both methods are associated with complications (*2*, *3*). For example, soft tissue autografts can help restore tissue form, but pain, seroma formation, wound breakdown, scar, and contour deformity might occur at the surgical site and where the tissue is harvested. Adipose grafts, in particular, suffer from inconsistent functional outcomes, although the addition of stem cells to lipoinjection has been suggested recently as a promising new strategy to improve engraftment (*4*). Biologically derived biomaterials can mimic some aspects of the native soft tissue extracellular matrix, but most biological molecules are susceptible to enzymatic degradation, thus reducing the material's functional efficacy and lifetime (*5*). Conversely, synthetic materials that do not degrade often cannot fully mimic the physical properties of native soft tissue, do not integrate well with surrounding tissues, and can elicit unwanted inflammatory responses (*5*).

The limitations of biological and synthetic materials have led to the development of composite materials that combine the benefits of biological activity while maintaining the mechanical strength and persistence of synthetic materials (*5*). Although biosynthetic composite materials are being studied intensely for bone and cartilage regeneration (*6*, *7*), investigation of their use in soft tissue reconstruction is limited (*8*). Clinical applications for injectable soft tissue augmentation have become popular for the treatment of skin contour defects secondary to aging (*9*), primarily with biological materials. For example, hyaluronic acid (HA) is an extracellular matrix molecule that contributes to dermal hydration and elasticity and is the basis for many commercially available temporary soft tissue replacements because of its physicochemical properties (*10*). Because HA is a biomolecule that exists naturally within the body, it can be rapidly degraded by hyaluronidases, which are enzymes normally found in the body. To compensate for this degradation and to extend implant lifetime and persistence of original shape after implantation, we used increased concentrations of HA and molecular crosslinking of the HA in soft tissue injections (*11*). Crosslinked HA is processed into particles so that the material can be injected through small-gauge needles for clinical application. Despite attempts to crosslink and use higher concentrations, HA materials have limited clinical persistence, thus requiring repeated application to maintain the desired effect (*12*). Furthermore, HA implant volumes are often insufficient for reconstruction of larger soft tissue defects, such as that required after tumor excision and trauma.

The ideal technology for soft tissue reconstruction would mimic the native extracellular matrix structure and function while integrating seamlessly into the surrounding host tissue. Furthermore, to facilitate clinical application, there must be control over the implantation process to manipulate elasticity and persistence of the desired reconstruction to maintain the original implant structure. To address these issues, we developed an approach for soft tissue

[1]Department of Otolaryngology, Johns Hopkins University, Baltimore, MD 21287, USA. [2]Translational Tissue Engineering Center, Wilmer Eye Institute and Department of Biomedical Engineering, Johns Hopkins University, Baltimore, MD 21287, USA. [3]Department of Ophthalmology, Stanford University, Palo Alto, CA 94305, USA. [4]Department of Chemical and Biomolecular Engineering, Johns Hopkins University, Baltimore, MD 21218, USA. [5]Energist North America, Nyack, NY 10960, USA. [6]Department of Radiology, Johns Hopkins University, Baltimore, MD 21287, USA. [7]Kythera Biopharmaceuticals, Calabasas, CA 91301, USA. [8]Department of Dermatology, Johns Hopkins University, Baltimore, MD 21287, USA.
*These authors contributed equally to this work.
†To whom correspondence should be addressed. E-mail: jhe@jhu.edu

reconstruction by combining widely available synthetic and biological materials and crosslinking the composite in situ with light.

RESULTS

A transdermally photoactivated composite implant

Our objective was to design a soft tissue reconstruction technology that could be implanted, manipulated into a desired shape, and then crosslinked with a controlled external stimulus (Fig. 1). Ideally, the approach should be universally applicable with respect to materials choice and should be able to integrate with current surgical and medical techniques. To accomplish this, we used light as an initiation mechanism to crosslink materials through skin. Light can penetrate tissue to varying degrees, with longer wavelengths reaching greater depths (*13*). A light-emitting diode (LED) was designed specifically to produce maximal tissue penetration by creating an array of diodes in a small handheld device (Fig. 2A) with an emission wavelength of 520 nm to closely match the absorbance of the common visible-light photoinitiator system of eosin Y, *N*-vinyl-2-pyrrolidone (NVP), and triethanolamine (Fig. 2B) (*14*). Penetration of the light through human abdominal skin is shown in Fig. 2C. With this combination of LED and photoinitiation system, light-induced crosslinking was possible through 4-mm sections of human pale white skin (Fitzpatrick type I: never tans, always burns) and olive skin (Fitzpatrick type III: sometimes tans, sometimes burns) types ex vivo (Fig. 2D). Light penetration of 1% through tissue depths of 4 mm of Fitzpatrick type III skin or lighter is adequate for injection and polymerizing implants for soft tissue replacement in most clinical craniofacial settings (*15*). In addition, the intensity of light emitted from the LED can be manipulated by altering the array design and the energy emitted to increase the depth of tissue penetration further for other applications.

The photosensitive crosslinking reaction progression was evaluated through and without skin by characterizing the material mechanical and swelling properties, which are directly related to the crosslinking of the hydrogels. The photosensitive prepolymer solution, placed in an ex vivo mold, was exposed to the custom LED light (43 mW/cm^2, 520 nm). As exposure time increased, the elastic modulus of the resulting material increased until 60 s, after which there was no longer a change in the material, thus confirming there was no further reaction or crosslinking (Fig. 2E). However, the photocrosslinking reaction might proceed slower under human skin and require longer light exposure. To maintain the clinical practicality of the implantation while maximizing depth of penetration, we selected a maximal light exposure time of 2 min for photocrosslinking implants through skin. Material crosslinking was evaluated under different skin samples in an ex vivo mold by measuring the swelling ratio, which is a function of crosslinking density and extent of photopolymerization. Photocrosslinking under 4-mm pale (type I) human skin was not statistically different from samples with less (<4 mm) or no skin (Fig. 2F); however, the reaction was less efficient under the darker (type III) human skin, as demonstrated by the increased swelling (decreased photocrosslinking) of the resulting materials (Fig. 2F).

To ensure safety of the transdermal photocrosslinking method, we applied LED light to living rodent skin for 2 min (Fig. 2G). No dermal or epidermal injury was noted. However, the light exposure produced a transient increase in local temperature of 2°C, as pictured in infrared imaging of the rat skin dorsum (Fig. 2H).

Formulation of biosynthetic composite material

The chemical composition and universal applicability of the soft tissue reconstruction technology was investigated. The photoinitiation system selected for crosslinking can react with any (meth)acrylate-containing polymer, including poly(ethylene glycol) (PEG) derivatives.

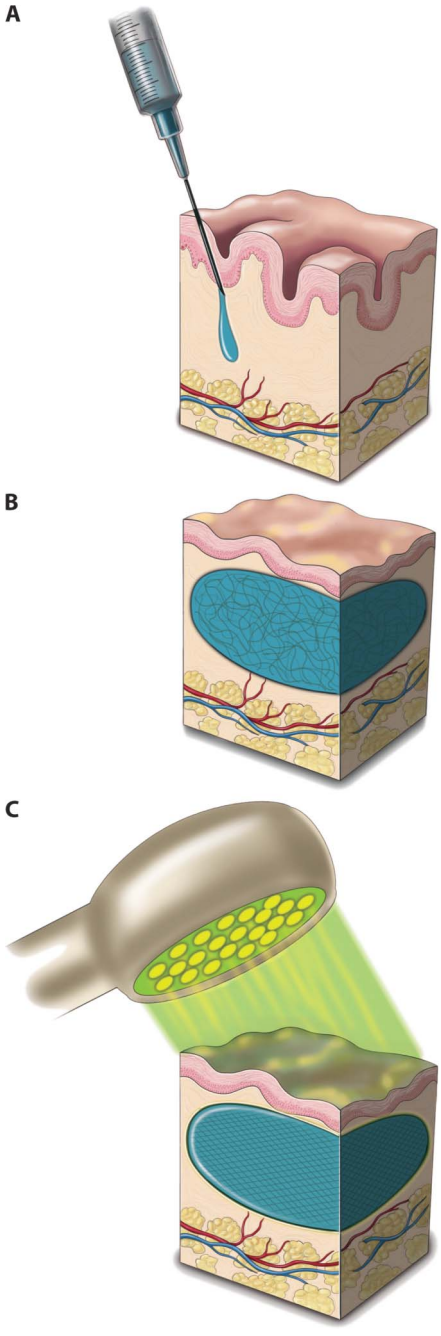

Fig. 1. Schematic showing transdermal photocrosslinking of composite soft tissue biomaterial. (**A**) Photopolymerizable poly(ethylene glycol) diacrylate–hyaluronic acid (PEG-HA) formulation is injected into the dermis. (**B**) The uncrosslinked solution (unorganized lines) is massaged into the desired shape. (**C**) Light-induced transdermal crosslinking to form the PEG-HA composite implant (organized lines).

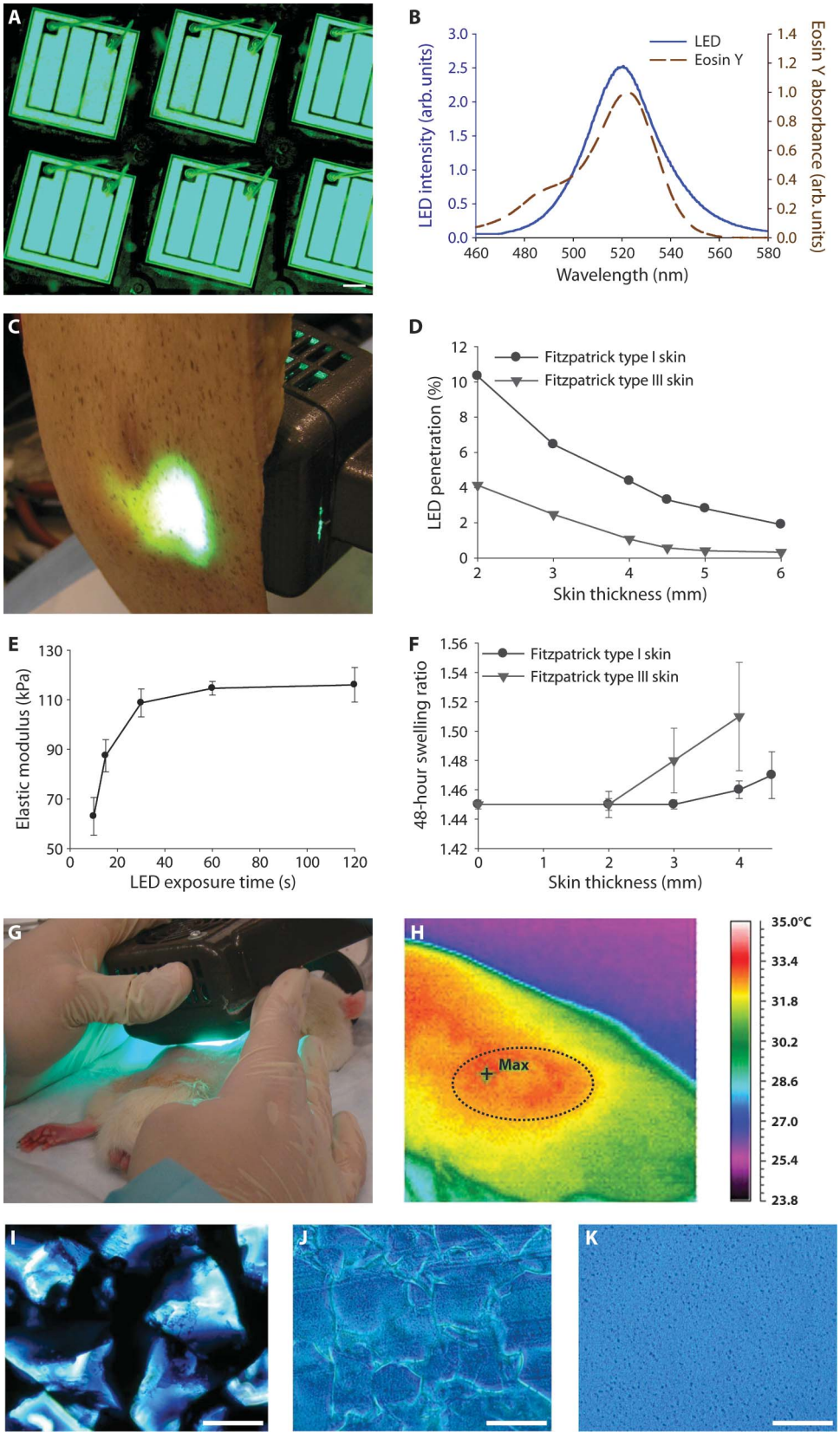

Fig. 2. LED design, skin transmission, and PEG-HA crosslinking. (**A**) A unique 520- to 530-nm light-emitting diode (LED) array was designed. Scale bar, 200 μm. (**B**) The LED emission wavelengths were closely matched with the absorbance of the eosin Y photoinitiation system. (**C**) The array was designed to maximize light penetration through human skin for photocrosslinking the PEG-HA material. (**D**) The LED array was able to penetrate at least 4 mm into Fitzpatrick types I (pale white) and III (olive) human skin. (**E**) LED exposure time at an intensity of 43 mW/cm^2 was tailored to maximally polymerize the PEG-HA system, as measured by a plateau in elastic modulus. Data are means ± SEM (n = 4). (**F**) Swelling of PEG100-HA20 after 48 hours that had been crosslinked through different thicknesses of Fitzpatrick types I and III human skin. Data are means ± SEM (n = 3). (**G** and **H**) LED exposure of injected composites in the rat dorsum was followed immediately by thermal imaging of implants (outlined). (**I** and **J**) Microscopic images of HA5 particles (stained with blue ink for contrast) before (I) and after (J) photocrosslinking with PEG100. Scale bars, 200 μm. (**K**) Unmodified linear HA (10 mg/ml, 980 kD) crosslinked with PEG100. Scale bar, 200 μm.

(Meth)acrylated PEG polymers have been used in several medical applications, such as lung and dural sealants, and the polymer is considered to be biocompatible because it does not induce severe inflammatory reactions (*16*, *17*). HA was selected as the biological component of the composite system owing to its viscous properties that enable injection and contouring, and recent clinical success as a temporary soft tissue replacement (*9*). Current clinically used HA formulations include both linear and crosslinked HA at various concentrations (*18*–*20*). Although linear, uncrosslinked, and low-concentration HA provides a smooth injection amenable to superficial placement, the material quickly degrades and diffuses away. Conversely, the particulate, crosslinked HA is too coarse for very superficial injections but is amenable to intradermal or subcutaneous implantation and has a longer in vivo lifetime. PEG alone can be injected as a liquid before in situ crosslinking; however, the solution has extremely low viscosity and diffuses away before crosslinking, such that no three-dimensional implant can be created. In addition, hydrogels

derived from PEG alone are brittle. The addition of HA to PEG increases the elasticity of the polymeric material to better match that of native soft tissue (table S1) (*5*–*7*).

PEG crosslinking occurs via acrylate groups on the ends of the polymer chains that react with photoinitiators and undergo radical polymerization. When the PEG polymer polymerizes and crosslinks to form a hydrogel, the HA molecules or particles are physically entrapped in the network. The nonspecific nature of radical reactions makes it possible that the PEG can crosslink with HA; however, this would likely only occur at very low levels, if at all. After photocrosslinking a solution containing PEG and crosslinked particulate HA, HA particles are embedded in the PEG hydrogel, and the interface between the HA particles and the bulk hydrogel is reduced, which suggests some interpenetration between the PEG and the crosslinked HA particulates (Fig. 2, I and J). Figure 2K shows the appearance of homogenous hydrogels when unmodified linear HA (10 mg/ml, 980 kD) is crosslinked with PEG. These results suggest that both crosslinked and uncrosslinked HA formulations form interpenetrating networks with PEG.

The crosslinking density and physical properties of the hydrogels were influenced by the percentage of PEG as well as the concentration and crosslinking of HA (Table 1 and table S2). Swelling of PEG hydrogels without HA correlated directly with the crosslinking density when evaluating the ratio of equilibrium wet weight to dry weight (*21*). As the amount of PEG increased, the crosslinking density also increased, creating a tighter network. In addition to comparing the standard swelling ratio of wet to dry weights (ww/dw), we also measured swelling by evaluating the hydrogel weight after 48 hours of swelling to equilibrium in saline and comparing to post-polymerization weight determined immediately after crosslinking. This clinical swelling ratio (ww/ww) estimates how much a hydrogel might swell after injection and polymerization. Characterizing such swelling ratios (table S2) can help one to understand how much a hydrogel might swell after injection and polymerization in vivo. The wet-to-wet swelling ratio of PEG gels in saline did not change significantly with PEG concentration, ranging from 0.9945 for PEG40 to 1.017 for PEG100 (a ratio of 1 would indicate no swelling), although the ww/dw swelling ratio confirmed a difference in overall crosslinking density (table S2). The swelling of the PEG hydrogels increased with the addition of HA, likely because of the strong hygroscopic nature of HA. Reducing the PEG content of PEG-HA hydrogels increased the clinical swelling further; swelling of the PEG40-HA5 hydrogel was significantly higher than its respective PEG100 hydrogels ($P < 0.05$), whereas PEG40-HA20 and PEG40-HA24 swelling could not be measured in vitro because the hydrogels became extremely fragile due to high swelling, therefore were difficult to accurately measure after 48 hours (table S2). Although increased ww/ww swelling was observed for the lower-dose PEG40-HA5 compared to PEG100-HA5, the mechanical properties were weaker. This indicates that in vitro swelling might not always correlate with in vivo swelling, where the mechanical tension of the skin is a counter force that will need to be considered.

Rodent implantation and PEG dose response

A rodent model was used to evaluate the PEG dose response in the composite PEG-HA implants and maintenance of volume or persistence. For the purposes of these studies, we defined persistence as the maintenance of the original implant volume after injection. A range of PEG concentrations were tested in combination with HA to create an implant system with tunable properties (Table 1). Photocrosslinkable implants containing greater than 20 mg of PEG were able to form gels in vitro with all concentrations of crosslinked HA (5, 20, and 24 mg/ml). PEG-HA formulations were injected subcutaneously and then photocrosslinked in situ with transdermal light for 2 min. The control implant was the corresponding HA alone. PEG injections without HA did not have adequate viscosity to create a discrete implant that could be polymerized in situ, so this control could not be tested in vivo. After LED exposure, the dimensions of the implant were measured with a caliper at multiple time points. Implant volume (mm^3) was calculated by assuming an ellipsoid shape as determined visually and by magnetic resonance imaging (MRI). About 200 μl of polymer was injected for each formulation, producing implants with initial measured volumes ranging from 77 to 126 mm^3 and initial measured heights ranging from 2.4 to 3.8 mm. The HA formulations contain both crosslinked and uncrosslinked HA to lubricate injection. The uncrosslinked HA quickly diffused from the implant site, leading to a smaller implant volume compared to injection volume. The lower-concentration HA control injections also quickly diffused from the implant site, which resulted in lower initial measured volumes, whereas higher-concentration HA (discussed subsequently) maintained its initial volume.

The addition of varying amounts of PEG (0, 20, 40, or 100 mg) to HA (5.5 mg/ml) improved volumetric persistence in a dose-dependent manner (Fig. 3A), with the PEG100-HA5 composite showing the greatest persistence and maintenance of 59% of the initial implant volume (91.3 mm^3) at 9 months. At the same time point, PEG40-HA5 and PEG20-HA5 retained 40% and 14% of their original volume, respectively, which was significantly greater than the in vivo control, even though they could not form discrete hydrogels in vitro. Unmodified control HA (0 mg PEG) resorbed the fastest (at 9 months) (Fig. 3A). Of particular importance in soft tissue reconstruction is maintaining the height of the implant because the tension of the skin pushes on the implant. The photocrosslinked PEG-HA maintained the original implantation height better than control implants (0 mg of PEG) (fig. S1A). Maintenance of initial height as well as initial volume was a function of increased PEG concentration in the PEG-HA gels, with the PEG100-HA implants showing the greatest persistence (Fig. 3 and fig. S1).

Comparison of PEG-HA with clinical HA formulations in rat

Next, we evaluated the effects of different HAs in combination with PEG100 that showed the greatest persistence or volume maintenance in the dose response studies. Given the limited persistence

Table 1. HA and PEG combinations in photopolymerizable composites.

Formulation	HA concentration (mg/ml)	PEG amount (mg)
HA5	5.5	—
HA20	20	—
HA24	24	—
PEG20-HA5	5.5	20
PEG40-HA5	5.5	40
PEG100-HA5	5.5	100
PEG100-HA20	20	100
PEG100-HA24	24	100

of most commercially available dermal HA injections, we evaluated the potential for photocrosslinking to increase the persistence. Current clinically used HA injections contain a range of concentrations and HA crosslinking. Several HA materials with low and high concentrations were evaluated (Table 1). These HA control injections are materials that are used in humans, so the results can be correlated to clinical experience. Implants were injected into the subcutaneous space on the dorsal surface of the rat. Volumetric analysis was performed immediately after photocrosslinking and periodically until control implants could no longer be detected (>210 days). Lifetime of control implants ranged from 210 to 491 days, depending on the HA formulation tested. The photocrosslinked PEG-HA composite implants maintained a significantly greater average volume (Fig. 3, B to D) and height (fig. S1, B to D) than their respective HA-only controls. Clinicians observe persistence as being a function of HA concentration and crosslinking (*22*); however, when HA is combined with PEG, there was no observable difference in persistence trends between high- and low-concentration HA. Because the low-concentration HA is resorbed relatively quickly, incorporation of PEG had the greatest impact on extending their lifetime. The addition of PEG also significantly increased persistence of the higher-concentration HA formulations (Fig. 3D and fig. S1D).

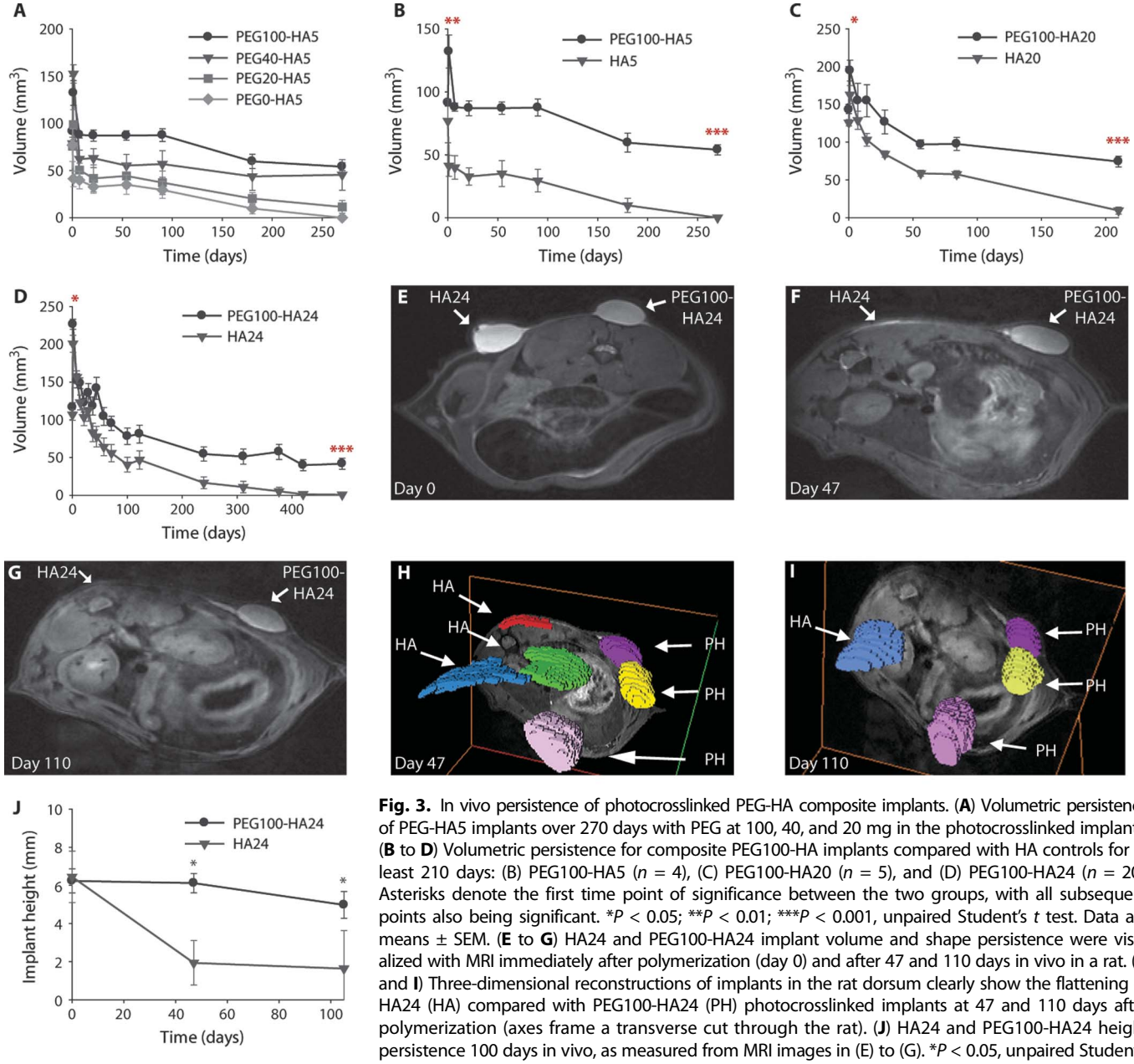

Fig. 3. In vivo persistence of photocrosslinked PEG-HA composite implants. (**A**) Volumetric persistence of PEG-HA5 implants over 270 days with PEG at 100, 40, and 20 mg in the photocrosslinked implants. (**B** to **D**) Volumetric persistence for composite PEG100-HA implants compared with HA controls for at least 210 days: (B) PEG100-HA5 (n = 4), (C) PEG100-HA20 (n = 5), and (D) PEG100-HA24 (n = 20). Asterisks denote the first time point of significance between the two groups, with all subsequent points also being significant. *P < 0.05; **P < 0.01; ***P < 0.001, unpaired Student's t test. Data are means ± SEM. (**E** to **G**) HA24 and PEG100-HA24 implant volume and shape persistence were visualized with MRI immediately after polymerization (day 0) and after 47 and 110 days in vivo in a rat. (**H** and **I**) Three-dimensional reconstructions of implants in the rat dorsum clearly show the flattening of HA24 (HA) compared with PEG100-HA24 (PH) photocrosslinked implants at 47 and 110 days after polymerization (axes frame a transverse cut through the rat). (**J**) HA24 and PEG100-HA24 height persistence 100 days in vivo, as measured from MRI images in (E) to (G). *P < 0.05, unpaired Student's t test. Data are means ± SEM.

Shape maintenance, as determined by initial and final implant heights, increased with PEG photocrosslinking for all HA concentrations. As expected, incorporation of the photocrosslinked PEG increased height persistence significantly for HA5 (from days 1 to 270; fig. S1B). PEG photocrosslinking of the higher-concentration HA formulations (HA20 and HA24) also resulted in improved shape maintenance over the course of 210 and 491 days, respectively (fig. S1, C and D). The height and volume persistence trends of the PEG100-HA photopolymerized implants were consistent across all HA types to a minimum time point of 210 days (Fig. 3 and fig. S1).

Implant volumetric analysis with caliper measurements and the photocrosslinking shape persistence was further validated in the rat model by MRI. Images of PEG100-HA24 and HA24 immediately after injection and photocrosslinking appeared similar in shape and size on day 0 (Fig. 3E). After 47 and 110 days, MR images demonstrated little change in the PEG100-HA24 implant appearance, whereas the control HA24-only injections had a decreased volume and undefined shape (Fig. 3, F and G). Three-dimensional volumetric reconstruction of implants in the rat dorsum at days 47 and 110 clearly demonstrated the loss of volume in the HA24 implants over time (Fig. 3, H and I), especially the height parameter, compared with the photocrosslinked composite implants (Fig. 3J). These MRI results further support the enhanced persistence of PEG-HA composite implants.

Implants are reversible with hyaluronidase in vivo

For the clinical utility of a semipermanent implant system, reversibility represents a crucial design component to allow correction of improper placement or migration. Hyaluronidase can reduce implants by breaking down both crosslinked and linear HA. For PEG-HA composites, only the HA portion of the implant is sensitive to enzymatic degradation. Photocrosslinked PEG-HA5 implant volumes and heights were partially reversible by an initial 150-μl hyaluronidase injection (200 U/ml) in a PEG dose–dependent manner (fig. S1, E and F). A second 150-μl hyaluronidase injection was performed 30 days later, resulting in further volumetric reduction by day 31 (fig. S1E). The height component of the implant also decreased significantly 24 hours after hyaluronidase treatment (fig. S1F). It is possible that implant height would show greater reversibility than volume. This height reversibility would likely be secondary to the elastic tension of the skin deforming the height, particularly if the implants were weakened by digestion of the HA portion of the composite. The higher PEG content materials (PEG100-HA20) showed no immediate response to the first or second hyaluronidase enzyme injection (fig. S1, G and H), but substantial loss of implant volume (Fig. 3G) and height (fig. S1H) occurred after 12 months compared with unexposed implants.

Implant rheological properties

Clinically, it is often desirable to match the properties of a biomaterial implant with the surrounding tissue. The mechanical effect of incorporating PEG with HA was evaluated on a parallel plate rheometer and compared to literature values for tissue samples (table S1). Unmodified HA20 produced an elastic modulus (G′) of 0.163 kPa, which was significantly lower than that of human skin (0.362 kPa) and adipose tissue (14.5 kPa) ($P < 0.0001$) (table S1), indicating that HA20 is a weak substitute for these soft tissues. The elastic modulus of PEG-HA20 composites increased in a PEG dose–dependent manner, with PEG10-HA20 (11.7 kPa) approaching that of adipose tissue (table S1). Rheological measurements likely overestimate G′ in adipose tissue owing to substantial compression that mechanically extracted lipids (*23*). Nonetheless, PEG100-HA20 exhibited the closest complex modulus to that of human adipose tissue, supporting the choice of PEG100 in formulations chosen for further studies.

Biocompatibility of photocrosslinked PEG-HA implants in the rat

The immunological response of the rats to both a high-concentration (PEG100-HA20) and a low-concentration (PEG100-HA5) HA formulation was evaluated at multiple time points (Fig. 4). At day 2, photocrosslinked PEG100-HA20 and HA20 demonstrated implants deep to the superficial dorsal muscle surrounded by an inflammatory pseudocapsule about 4 to 6 cell-layers-thick. The PEG100-HA20 had a thicker infiltrate densely populated by neutrophils, characteristic of acute inflammation. At 1, 5, and 15 months, PEG100-HA5 implants had a reduced inflammatory response with pockets of neutrophils and focal areas of macrophages with rare multinucleated giant cells. The PEG100-HA5 implants had an acute and chronic inflammatory response compared with minimal inflammation surrounding the HA5 control implants. A PEG dose–dependent phenomenon is noted at 15 months, with PEG100-HA5 showing the least amount of cell infiltration and improved shape persistence, whereas PEG40-HA5, PEG20-HA5, and HA5 showed progressively more adjacent tissue invasion. At 18 months, the PEG100-HA20 implant demonstrated a reduced acute and chronic inflammatory response compared to earlier time points (the corresponding HA20 implant had been resorbed by this time). Overall, there was slightly more inflammation seen surrounding PEG-HA implants compared to HA controls, but this difference was minimal and was consistent with a foreign body response (Fig. 4). Gram-Weigert and Brown and Hopps stains for bacteria were negative in all samples (fig. S2).

HA increases type I collagen production

Local tissue remodeling and collagen deposition were present near PEG-HA and HA materials implanted in the rodent (fig. S3), suggesting that these biomaterials might have some permanent effects on the local tissue organization and volume. The potential of the PEG-HA composites and HA implants to influence in vivo local tissue remodeling and extracellular matrix production was characterized in a simplified in vitro system. Specifically, the effect of unmodified linear HA on fibroblast production of type I collagen was evaluated and compared with the addition of chondroitin sulfate (CS)—another extracellular matrix polysaccharide. Immunohistochemistry demonstrated increased staining for procollagen in the fibroblasts cultured in vitro with HA (1 and 5 mg/ml) (fig. S3A) compared with cells cultured in standard medium (fig. S2B). Gene expression analysis of cultured fibroblasts revealed a trend toward up-regulation of *type I collagen* in the presence of 1 mg/ml HA compared with 5 mg/ml CS and standard medium controls (fig. S3C) after 4-day culture in HA-supplemented medium. Furthermore, there was a trend toward increased fibroblast expression of *transforming growth factor–β1* (*TGF-β1*) and *TGF-β3* with the addition of HA compared to CS and standard medium controls (fig. S3, D and E). *TGF-β3* has been found to increase in vitro fibroblast motility along with decreasing wound scarring (*24*, *25*). Therefore, up-regulation of *TGF-β3* expression via HA exposure may result in increased remodeling around the implant site while reducing scar tissue formation.

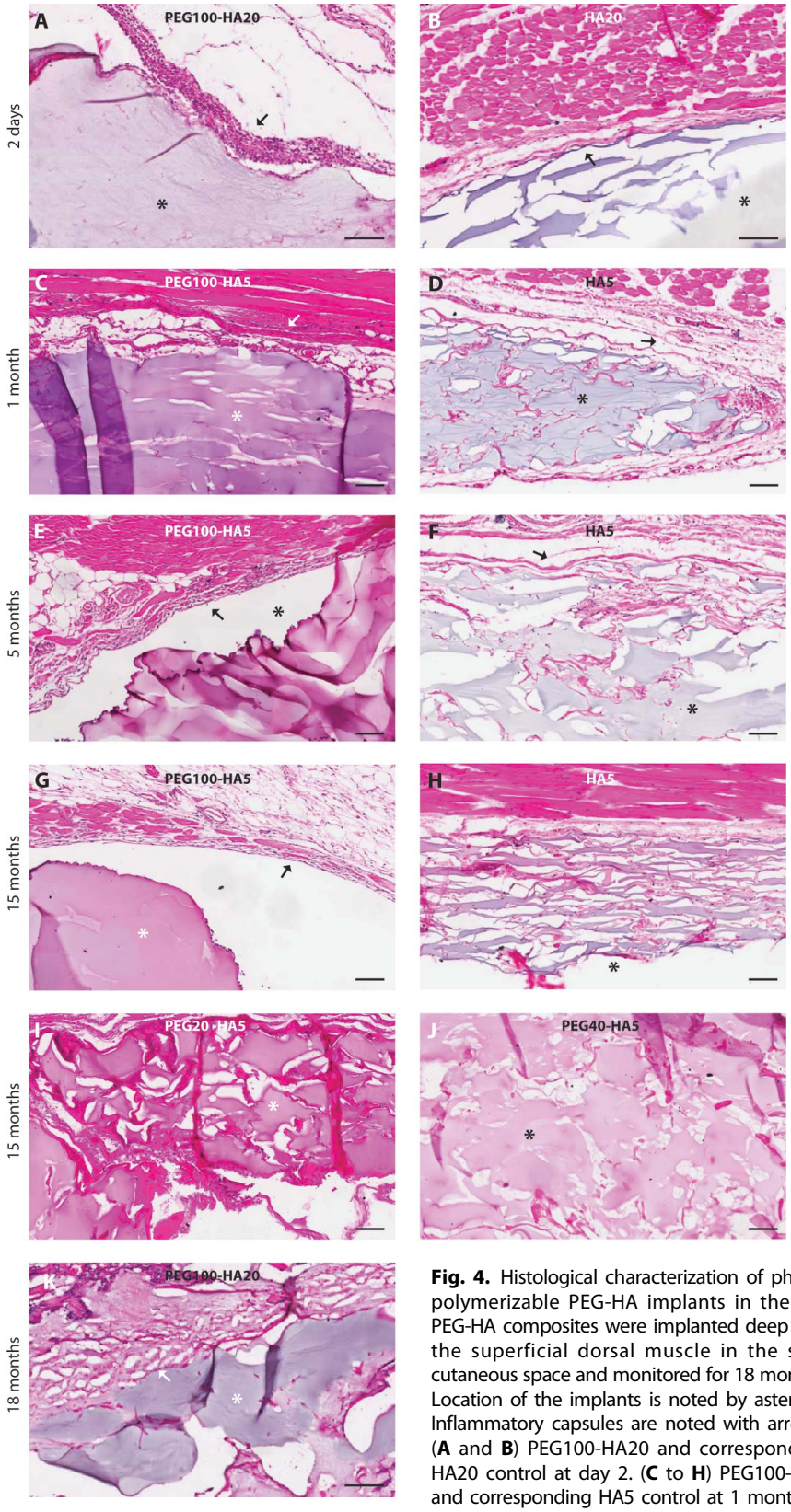

Fig. 4. Histological characterization of photopolymerizable PEG-HA implants in the rat. PEG-HA composites were implanted deep into the superficial dorsal muscle in the subcutaneous space and monitored for 18 months. Location of the implants is noted by asterisks. Inflammatory capsules are noted with arrows. (**A** and **B**) PEG100-HA20 and corresponding HA20 control at day 2. (**C** to **H**) PEG100-HA5 and corresponding HA5 control at 1 month (C and D), 5 months (E and F), and 15 months (G and H). (**I** and **J**) PEG20-HA5 and PEG40-HA5 are shown at 15 months. (**K**) PEG100-HA20 was followed until 18 months in vivo. Scale bars, 100 μm.

Pilot clinical testing comparing photocrosslinked PEG100-HA and HA implants

A 12-week pilot clinical trial was initiated to evaluate the safety and efficacy of the photocrosslinked PEG-HA compared to commercial HA implants. The PEG100-HA formulations were chosen on the basis of greatest observed volume maintenance in the rodent studies. The two HA formulations, HA20 (n = 12) and HA24 (n = 12), were selected because of their widespread clinical use and compared with PEG100-HA20 (n = 12) and PEG100-HA24 (n = 12). Injections (250 μl) were placed into the intradermal and subcutaneous space of patients (n = 3) 12 weeks before scheduled abdominoplasty surgery. There were no serious adverse events, including fatalities, hospitalization, disability, or reactions resulting in any significant medical hazard, with the PEG100-HA20 and PEG100-HA24 implants or the controls. Mild transient erythema and sensation of heat and pain during light exposure during photocrosslinking of dermal implants were noted but were all resolved within 12 hours of crosslinking. MR images of the PEG100-HA24 and HA24 implants were similar upon injection into the subcutaneous space at day 0 (Fig. 5A). On the basis of post-abdominoplasty histological analysis, implant location was principally subdermal, surrounded by adipose tissue with some extension into the deep intradermal space. MRI of the photocrosslinked PEG100-HA24 composite implants demonstrated maintenance of shape over the 12 weeks of implantation compared with HA24 injections that flattened and exhibited a qualitative decreased T_2 intensity (Fig. 5A). Quantification of the MR images after days 1 and 84 showed that the HA implants experienced a significant loss of height ($P < 0.05$). HA20 and HA24 control injections maintained only 50% and 77% of their original height, respectively (Fig. 5B). In comparison, the PEG100-HA20 and PEG100-HA24 implants maintained 100% of the original injection height (7.1 and 8 mm, respectively) after 12 weeks.

Implants were retrieved after abdominoplasty at week 12 and stained with hematoxylin and eosin (H&E) (Fig. 6). Subsequently, immunohistochemical analysis of CD3, CD4, CD8, and CD20 was performed on HA control implants (HA24, n = 1; HA20, n = 1) and PEG-HA composite implants

(PEG100-HA20, $n = 1$; PEG100-HA24, $n = 1$) to further characterize the immune response (Fig. 6). HA20 and HA24 control implants showed a range of inflammatory responses, with 9 of 28 implants demonstrating a mild to moderate chronic inflammatory response (histiocytes, lymphocytes, and giant cells) on H&E stain; HA20 represented 6 of the 9 samples. One control also demonstrated an acute inflammatory infiltrate (neutrophils). HA24 implants did not stain positive for CD3, CD4, CD8, or CD20 immune cell surface markers. However, the HA20 sample demonstrated a chronic inflammatory pseudocapsule 5 to 20 cell-layers-thick (Fig. 6), composed predominantly of histiocytes with scattered (about 1 in 20 cells) T lymphocytes, highlighted by CD3 immunostaining. Further evaluation of the T lymphocytes infiltrating the HA20 material revealed a mixed population of CD4 and CD8 lymphocytes, with a slight CD8 predominance, suggesting a mixed cytotoxic and helper T cell response. There were no $CD20^+$ B lymphocytes present in the HA20 implant.

A similar pattern of inflammatory response was found in the composite PEG100-HA24 and PEG100-HA20 implants (Fig. 6), generally with greater chronic inflammation. An implant pseudocapsule around the composite implants was observed with variable thickness, as evidenced by the 4 to 6 cell-layer-thick pseudocapsule surrounding the PEG100-HA24. Six of the 32 PEG-HA composite samples also showed neutrophils superimposed with the histiocytes and T lymphocytes. Specifically, both $CD3^+$ T lymphocytes and $CD20^+$ B lymphocytes were identified alongside a neutrophilic and fibrous capsule surrounding the PEG100-HA20.

Although some neovascularization was present in parts of the capsular tissue of the composite and HA implants, there was no vascularization (Fig. 6). Gram-Weigert and Brown and Hopps stains for bacteria were negative in all composite samples (fig. S2), thus indicating a lack of infection around the implants. For many of the samples, the inflammatory process appeared to be connected to the adjacent adipose tissue, which indicates adipose tissue's potential influence on the inflammatory response. This is particularly relevant in an abdominoplasty model where significant fat tissue is present depending on the implant location in the intradermal or subdermal space. In addition to the influence of implant location and chemical differences between the HA and the PEG-HA formulations, their rheological properties also differ substantially, which might affect mechanical interactions with the skin, subdermal space, and adipose tissue, to cause irritation.

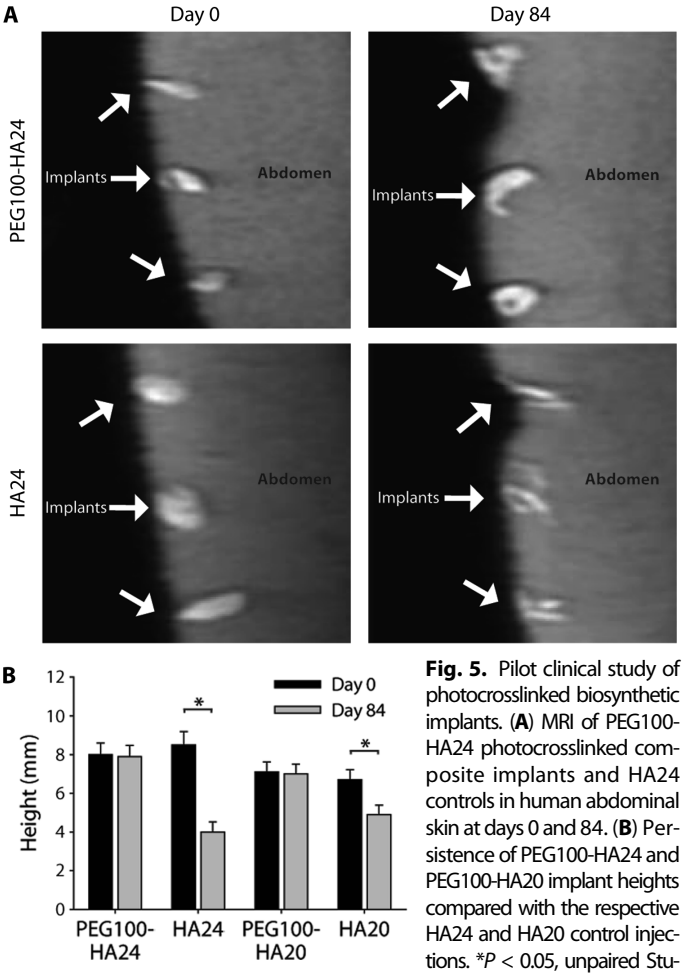

Fig. 5. Pilot clinical study of photocrosslinked biosynthetic implants. (**A**) MRI of PEG100-HA24 photocrosslinked composite implants and HA24 controls in human abdominal skin at days 0 and 84. (**B**) Persistence of PEG100-HA24 and PEG100-HA20 implant heights compared with the respective HA24 and HA20 control injections. *$P < 0.05$, unpaired Student's t test. Data are means ± SEM ($n = 12$).

DISCUSSION

The goal of this work was to design and optimize a flexible, biosynthetic, soft tissue replacement system that is compatible with any HA formulation, with customizable viscoelastic properties and controllable residence time in vivo. Photopolymerizable PEG was chosen because of its ability to crosslink and entangle HA, its hydrophilic compatibility, and titratable effects on the composite implant. Furthermore, the physical properties of the composite implants could be modified as a function of PEG and HA concentration (table S2). PEG-HA composites could be injected as a viscous prepolymer material and photocrosslinked in situ to create a semipermanent implant. In addition, our results highlight the versatility of the synthetic component as an additive to HA, because the composite PEG-HA maintained reversibility and demonstrated enhanced persistence.

The adaptability of the PEG-HA photocrosslinked soft tissue implant system was demonstrated in its consistency of results with different HA formulations, the dose-dependent effect of PEG concentration, and reversibility with hyaluronidase. As the amount of synthetic PEG increased, PEG-HA implant persistence increased and enzymatic degradation by hyaluronidase decreased (fig. S1, E to H). As demonstrated in our preclinical studies, the higher-concentration PEG100-HA20 and PEG100-HA24 materials had increased persistence when compared with the respective HA controls and the lower-concentration PEG-HA composites. Nevertheless, incorporating PEG with the lower-dose HA5 had a significant impact on extending persistence. Combining higher-concentration HA20 and HA24 with the optimum PEG concentration for different applications must take into account both the mechanical behavior of the material and the desired longevity to tailor a material that closely mimics the host tissue properties. The lower-concentration HA formulations are amenable to more superficial injections, so the PEG-HA5 formulations would also be most relevant for those applications. For example, a low–PEG dose, high-elasticity PEG-HA implant, such as PEG40-HA24 or PEG40-HA20, might be used as a dermal injection for nasolabial fold lines. Conversely, a high–PEG dose, low-elasticity PEG-HA implant, such as PEG100-HA24 or PEG100-HA20, might be used for supraperiosteal malar or mental injections that tolerate a firmer implant with longer-

lasting results. Moreover, should there be overinjection, implant migration, or improper placement, reversibility provides a considerable margin for patient safety as we demonstrated that PEG-HA was reversible with hyaluronidase, even at higher PEG quantities (PEG100) (*26*).

The versatility in the photocrosslinked composite implant design translates to multiple clinical applications. Furthermore, the current formulation of PEG-HA could be modified to host differentiated or stem cells to enhance local regeneration after injection. Both PEG and HA have demonstrated success as a scaffold, with photopolymerization of PEG scaffolds successfully involved in producing chondrogenic and adipogenic regeneration (*27*–*30*). As demonstrated by Yoshimura *et al.*, treatment of facial lipoatrophy with a progenitor cell supplement to autotransplanted adipose tissue can enhance clinical outcomes (*4*). A cellular component could potentially regenerate local tissues, whereas the photopolymerized composite is resorbed. Additionally, endoscopic applications would allow access to several other locations, including the pharynx, larynx, and gastrointestinal and genitourinary tracts, with activation via transmucosal application of light.

Dermal injections derived from biological molecules might have application as a stimulator of collagen to aid in local tissue remodeling (*9*). Mechanical tension is one mechanism that has been suggested to cause fibroblast stretching with subsequent increased collagen synthesis when HA is injected (*9*). Our results in fig. S3 support an additional biological basis for HA stimulation of enhanced collagen production by fibroblasts. We found that in vitro exposure of fibroblasts to HA stimulated *type I collagen* expression and increased *TGF-β1* and *TGF-β3* gene expression compared with controls and a different extracellular matrix molecule, CS. Combined with histological evidence of increased collagen deposition, this finding suggests that local fibroblasts produce new tissue in response to HA. Both TGF-β1 and TGF-β3 are growth factors that contribute to wound healing, and their enhanced expression in response to HA exposure suggests potential structural changes in the dermis (*31*).

The PEG-HA formulations that demonstrated the greatest volume persistence in the rodent preclinical studies were then used in human abdominal injections so that local tissue immune response could be evaluated after abdominoplasty. PEG-based materials have a record of biocompatibility (*16*, *17*, *32*); however, the inflammatory response to the PEG-HA implants in the human clinical trial was generally greater than that observed around the HA controls, and it demonstrated a different balance in acute and chronic inflammation as appreciated in the small animal studies. Potential reasons for the increased inflammatory response include species-specific differences (rat versus human), chemical aspects of the PEG, mechanical properties of the PEG-HA materials, and/or location of implant. In particular, the human implants placed in the abdomen were surrounded by relatively large amounts of adipose

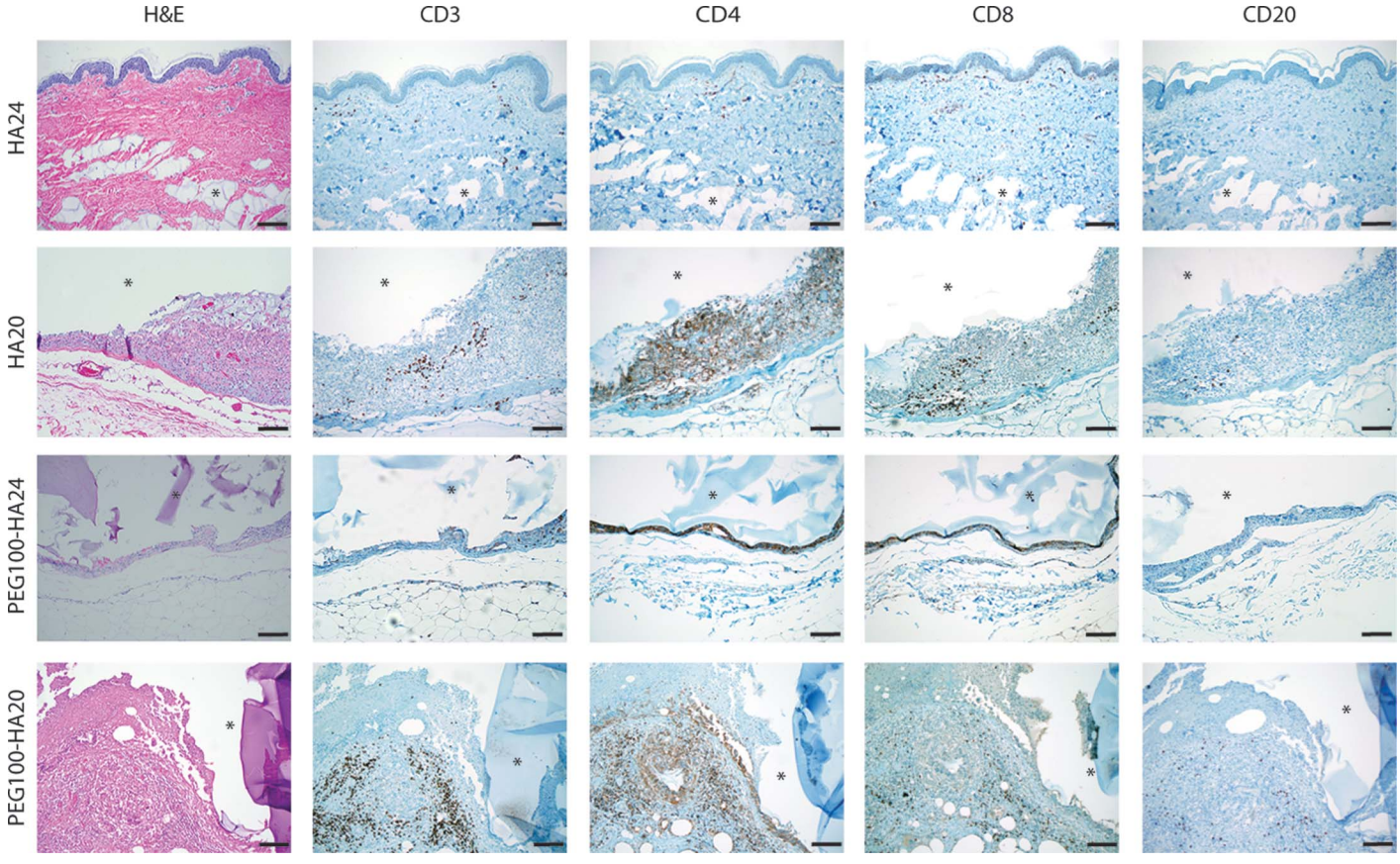

Fig. 6. Immune response to implants in humans. PEG100-HA implants were examined ex vivo after 12 weeks. Representative images are shown for the composite implants (n = 32) as well as HA controls (n = 28). H&E shows tissue morphology, including the presence of pseudocapsules and inflammatory cells. Inflammatory cells were further characterized by immunostaining for T lymphocytes (CD3), helper T cells (CD4), cytotoxic T cells (CD8), and B lymphocytes (CD20). In all images, an asterisk denotes the implant location. Scale bars, 100 μm.

tissue, which was not present near the rodent implants. This difference in the local environment and potential adipokine activation might play a role in inciting or augmenting an inflammatory response (*33*). The various tissue types present around an implantation site might also affect the mechanical integration or matching with the implants. For instance, the PEG100-HA20 formulation was an order of magnitude more rigid compared to human skin and probably more rigid than adipose tissue when lipids are included in the tissue (table S1). This mechanical mismatch in the local tissue environment might induce irritation and inflammation, which is particularly relevant in an abdominal model where the implants may be exposed to a number of mechanical forces. Finally, only PEG100-HA implants were assessed clinically; therefore, it is possible that lower PEG concentrations may attenuate the inflammatory response.

The T lymphocytes and histiocytes surrounding the composite implants may be associated with either an allergic (immunological) response or a non-allergic foreign body response, inflammatory reactions that can be difficult to differentiate on histological analysis. Multinucleated giant cells represent the predominant finding in a non-allergic foreign body response; however, the inflammatory pattern in our human samples tended toward diffuse histiocytes with variable lymphocytes and scattered giant cells—a finding that supports an allergic etiology (*34*). Both PEG and HA implants have had reports of a granulomatous response, which are often seen around implants (*35*, *36*). Reaction patterns to commonly used implants, such as silicone (*37*), result in a foreign body reaction, whereas that seen with dermal fillers, such as collagen (*38*) and HA, also include eosinophils and neutrophils (*39*). In the drug delivery literature, the level of anti-PEG immunoglobulin M (IgM) antibody production depends on the compound combined with PEG (*40*, *41*). Here, the absence of plasma cells and B lymphocytes argues against an antibody-mediated reaction surrounding the implant. Furthermore, the photoinitiator has been tested clinically in lung and dural applications in combination with degradable PEG formulations without adverse events, thus suggesting that these small molecules are not highly toxic at low levels (*16*, *17*). Finally, recent evidence suggests that the nonadhesive nature of PEG materials might play a role in the inflammatory process and that this can be remedied through the incorporation of adhesive peptides, such as Arg-Gly-Asp (RGD) (*36*). Together, these results demonstrate the importance of considering implant location as well as physicochemical properties when formulating biomaterials, even when using what are considered to be highly biocompatible polymers.

Continued biomaterials development and application in different tissue environments is necessary to realize the full potential of the soft tissue replacement technology. For example, implantation in clinically relevant sites beyond the abdomen is required, using formulations with similar physical properties to the surrounding tissue environment. Nevertheless, our results present a photocrosslinkable biosynthetic material that might be customized to manipulate elasticity, persistence, and reversibility, resulting in multiple applications from superficial dermal injections to deep tissue injections and providing a new tool for craniofacial soft tissue contouring and reconstruction.

MATERIALS AND METHODS

Formulation of photocrosslinked PEG-HA implants

Photocrosslinked PEG-HA biosynthetic implants were formulated with commercial bacteria-fermented HA formulations at various concentrations: 5.5 mg/ml (HA5; Prevelle Silk, Mentor Corporation), 20 mg/ml (HA20; Restylane, Q Med), and 24 mg/ml (HA24; Juvéderm Ultra, Allergan Inc.). The HA formulations were combined with a photochemical concentrate containing an eosin Y photoinitiation system and PEG diacrylate. Varied amounts of PEG (3.4 kD, Sunbio) were combined with 69 μg of eosin Y disodium salt (Sigma), 20 μl of NVP (Sigma), and 30 μl of triethanolamine (Sigma) in 80 μl of phosphate-buffered saline (PBS; Invitrogen). The photochemical concentrate volume expanded to 220 μl and then was mixed thoroughly with 1 ml of a commercial HA. Photochemical concentrates contained 20 mg (16 mg/ml), 40 mg (33 mg/ml), and 100 mg (82 mg/ml) of PEG. PEG-HA photocrosslinkable materials were named by PEG content and HA concentration (Table 1).

The morphology of PEG-HA implants was analyzed by light microscopy. Thin films of HA5, PEG100-HA5, and photocrosslinkable concentrate containing linear HA (Lifecore Biomedical) were injected (100 μl) between two glass slides with a 0.25-mm Teflon spacer. After crosslinking exposure to 520 nm light at 43 mW/cm^2 for 1 min, the upper slide was removed and blue dye (Inkcraft) was added as a contrast agent. Images were taken with a Nikon Eclipse TE200 microscope fitted with a DXM 1200 digital camera and processed with ACT-1 image software (Nikon).

Light penetration through human skin

Fitzpatrick type I and type III human skin (Asterand) was uniformly shaved with a surgical blade to a thickness ranging from 2 to 6 mm. Skin samples were exposed to a custom-built 520-nm LED array (Energist North America). A radiometer (Gigahertz-Optik X9-7 with a RW-3703 visible light detector head) was used to measure the light intensity at each millimeter interval between 2 and 6 mm. The LED emission wavelength was matched with the known absorbance of the eosin Y photoinitiator (Fig. 2B).

PEG-HA implant persistence in rodents

Eight 8-week-old male Sprague-Dawley rats (Charles River) were obtained and animal procedures were approved by the Johns Hopkins University Animal Care and Use Committee. Rats were housed in single cages after surgery and had free access to food and water. Animals were induced with 2% isoflurane (Halocarbon) and maintained with 1.5% isoflurane using a tabletop anesthesia system (VetEquip Inc.). Dorsal fur was shaved with Golden A5 clippers (Oster Professional Products), and the remaining dorsal fur was removed with Nair Hair Remover cream (Church & Dwight Co.) applied to the dorsum for 3 min.

Tunability of the in vivo persistence of PEG-HA implants was assessed by varying the amount of PEG (20, 40, or 100 mg) combined with the photoinitiator and added to 1 ml of HA5. This was compared to control HA5 implants. Two hundred microliters of each formulation were injected (n = 5) into the dorsal subcutaneous space of a rat. Volumetric analysis was performed until the unmodified HA was completely resorbed.

To compare high-dose PEG100-HA persistence with HA controls, we subcutaneously injected animals with 200 μl of PEG-HA prepolymer formulations para-spinally along the dorsum of each rat. The formulations evaluated in vivo in rat were PEG100-HA5 (n = 4 implants), PEG100-HA20 (n = 5), and PEG100-HA24 (n = 20) compared with HA5 (n = 4), HA20 (n = 5), and HA24 (n = 20). Care was taken to ensure equal injection distance and consistent injection shape (via massage) in the rat skin. HA and PEG-HA implants were separated

in each animal by a distance of about 1 to 2 cm along the rostral-caudal plane of the animals. The prepolymer injection material was exposed transdermally to a 520-nm LED array (43 mW/cm^2) for 2 min. To assess heating during transdermal photocrosslinking, we obtained infrared images of the implant sites with a thermal camera (Raz-IR SX Pro, SPI Corp.) before and after LED exposure.

Implant volume and height were assessed over time by three-axis measurements with a digital micrometer (Mitutoyo). Implant volume was approximated as an ellipsoid ($V = 1/6\pi LWH$), where L is the length, W is the width, and H is the height after polymerization. Animals were shaved and the implants were measured along the three longest perpendicular axes. Measurements were carried out a total of three times at each time point and were obtained by a single observer to avoid intraobserver variability.

Implant imaging

In vivo animal MRI was performed on rats implanted with PEG100-HA24 and HA24 with a horizontal 9.4-T NMR spectrometer (Bruker Biospin) with a volume coil (70-mm diameter) as radiofrequency transmitter and receiver. Before and during imaging, rats were anesthetized with 1.5% isoflurane and a mixture of air and oxygen at 3:1 ratio. The respiratory rate was monitored and maintained at about 50 breaths per minute by adjusting the anesthetic concentration. Axial images of the rat body were acquired with a T_2-weighted fast spin-echo sequence with an echo time of 16 ms, a repetition time of 8500 ms, an echo train length of 4, 1-mm slice thickness, six signal averages, and an imaging resolution of 0.267 mm × 0.400 mm. The total imaging time for each rat was 30 min. Images were reconstructed on the spectrometer console and transferred to a personal computer workstation. Implant MR images were manually outlined with ROIeditor (X. Li, H. Jiang, and S. Mori, Johns Hopkins University, Baltimore, MD, http://www.mristudio.org), and volumes were calculated with Amira software (Visage Imaging).

Rodent implant histology

Histologic analysis of both high- and low-concentration HA implants was performed with H&E and analyzed with light microscopy. Gram-Weigert and Brown and Hopps staining for Gram-positive and Gram-negative bacteria was performed on rodent HA20 and PEG100-HA20 implants at day 2 after polymerization to verify location of the implantation and to evaluate inflammatory response. Subsequent histologic evaluation was performed with HA5 and PEG100-HA5 implants from rats at 1, 5, and 15 months. A PEG100-HA20 implant was harvested and analyzed at 18 months (the corresponding HA20 implant had been resorbed). One animal was euthanized at each time point. Implants were excised along with the overlying skin and underlying subcutaneous tissue and fixed in 4% formalin for 1 week. The tissue was transected through its central axis and embedded in paraffin. Sections were stained with H&E and analyzed with light microscopy. Digital photomicrographs were taken.

Implant rheological testing

Representative rheological properties of PEG-HA biomaterials were determined for PEG100-HA20 ($n = 4$) and PEG40-HA20 ($n = 4$). We used a high-concentration HA (20 mg/ml) to match one of the formulations used in the clinical trial. Small deformation oscillation dynamic rheological measurements were carried out with an RFS 3 rheometer (TA Instruments) fitted with a 7.9-mm parallel plate fixture and compared with human adipose tissue ($n = 4$) (IRBX #02-08-08-04E) and unmodified HA20 ($n = 4$). The use of a small plate was required to test the material. Oscillation measurements were made over a frequency range of 0.1 to 100 Hz at a strain rate found from the linear viscoelastic region of a dynamic strain sweep. Elastic modulus, G', was then calculated.

Human clinical trial

A 12-week, human-subject controlled experiment (IRB #143574 Health Canada) was designed to evaluate the safety and clinical persistence of intradermal and subdermal implants of HA20 ($n = 12$) and HA24 ($n = 12$) implants compared with PEG100-HA20 ($n = 12$) and PEG100-HA24 ($n = 12$) photocrosslinked implants. We injected 250-μl prepolymer into the abdominal skin of three patients 12 weeks before planned abdominoplasty. After injection with the composite material, the patient's abdominal skin was exposed to LED light to polymerize the material. Injection sites were designated with a fluorescent tattoo. Subjects were evaluated at day 1 and at weeks 4, 8, and 12. Evaluation involved MRI, physician physical examination (including abdominal skin and implant assessment), patient-performed abdominal skin survey, urinalysis, and blood serum analysis. The primary safety endpoint was the incidence rate of adverse events in subjects implanted with HA20 and HA24 compared with those implanted with PEG100-HA20 and PEG100-HA24 after 12 weeks. No patients were terminated early from the study.

Histologic analysis of human HA20, HA24, PEG100-HA20, and PEG100-HA24 implants was performed after abdominoplasty at 12 weeks after injection to verify location of the implant and to evaluate inflammatory response. Implants were excised with the overlying skin and underlying subcutaneous tissue and fixed in 4% formalin for 1 week. The tissue was transected through its central axis and embedded in paraffin. Sections were stained with H&E and analyzed with light microscopy. Gram-Weigert and Brown and Hopps staining for Gram-positive and Gram-negative bacteria was performed. Human paraffin-embedded specimens were cut into serial slices and mounted on SuperFrost Plus coated glass slides (Fisher Scientific) and air-dried. Slices were then deparaffinized, rehydrated, and underwent antigen retrieval (Dako target retrieval solution, high pH, S3307, autoclaved, 10 min; Dako). After cooling for 20 min at room temperature, decant retrieval solution was washed two to three times in room temperature with PBS solution. The primary antibody was added and the specimen was incubated at 4°C for 16 hours. Staining was performed with the Ventana autostainer (DAB detection kit; iVIEW, Ventana Medical Systems). The following anti-human monoclonal antibodies were used: CD3 (Leica Microsystems Inc.) to stain for T lymphocytes, CD4 (Cell Marque) to identify histiocytes and helper T lymphocytes, CD8 (Cell Marque) to identify cytotoxic T lymphocytes, and CD20 (Ventana) to stain for B lymphocytes. Digital photomicrographs were taken with an Olympus BX45 microscope fitted with an Olympus DP-72 digital camera and processed with XV Image Processing software (Olympus).

Statistical analysis

Data were analyzed with an unpaired, two-tailed Student's t test for volume and height of the PEG-HA and HA implants at each time point. A P value of less than 0.05 was considered to be statistically significant.

SUPPLEMENTARY MATERIAL

www.sciencetranslationalmedicine.org/cgi/content/full/3/93/93ra67/DC1
Materials and Methods
Fig. S1. PEG-HA composite materials maintain their shape in vivo.

Fig. S2. No bacterial infection was noted in rodent or human implants.
Fig. S3. Effect of HA on collagen production by human foreskin fibroblasts.
Table S1. Rheological characterization of PEG-HA and soft tissues.
Table S2. Swelling ratio and compression modulus of photocrosslinked PEG-HA fillers compared to a PEG-only control.
References

REFERENCES AND NOTES

1. E. Robinson, N. Rumsey, J. Partridge, An evaluation of the impact of social interaction skills training for facially disfigured people. *Br. J. Plast. Surg.* **49**, 281–289 (1996).
2. J. C. Lee, H. St-Hilaire, M. R. Christy, M. W. Wise, E. D. Rodriguez, Anterolateral thigh flap for trauma reconstruction. *Ann. Plast. Surg.* **64**, 164–168 (2010).
3. A. G. Salles, P. H. Lotierzo, R. Gemperli, J. M. Besteiro, L. C. Ishida, R. P. Gimenez, J. Menezes, M. C. Ferreira, Complications after polymethylmethacrylate injections: Report of 32 cases. *Plast. Reconstr. Surg.* **121**, 1811–1820 (2008).
4. K. Yoshimura, K. Sato, N. Aoi, M. Kurita, K. Inoue, H. Suga, H. Eto, H. Kato, T. Hirohi, K. Harii, Cell-assisted lipotransfer for facial lipoatrophy: Efficacy of clinical use of adipose-derived stem cells. *Dermatol. Surg.* **34**, 1178–1185 (2008).
5. D. Seliktar, Extracellular stimulation in tissue engineering. *Ann. N. Y. Acad. Sci.* **1047**, 386–394 (2005).
6. W. Wang, B. Li, Y. Li, Y. Jiang, H. Ouyang, C. Gao, In vivo restoration of full-thickness cartilage defects by poly(lactide-co-glycolide) sponges filled with fibrin gel, bone marrow mesenchymal stem cells and DNA complexes. *Biomaterials* **31**, 5953–5965 (2010).
7. M. W. Laschke, A. Strohe, M. D. Menger, M. Alini, D. Eglin, In vitro and in vivo evaluation of a novel nanosize hydroxyapatite particles/poly(ester-urethane) composite scaffold for bone tissue engineering. *Acta Biomater.* **6**, 2020–2027 (2010).
8. V. W. Wong, K. C. Rustad, M. G. Galvez, E. Neofytou, J. P. Glotzbach, M. Januszyk, M. R. Major, M. Sorkin, M. T. Longaker, J. Rajadas, G. C. Gurtner, Engineered pullulan-collagen composite dermal hydrogels improve early cutaneous wound healing. *Tissue Eng. Part A* **17**, 631–644 (2011).
9. F. Wang, L. A. Garza, S. Kang, J. Varani, J. S. Orringer, G. J. Fisher, J. J. Voorhees, In vivo stimulation of de novo collagen production caused by cross-linked hyaluronic acid dermal filler injections in photodamaged human skin. *Arch. Dermatol.* **143**, 155–163 (2007).
10. F. Duranti, G. Salti, B. Bovani, M. Calandra, M. L. Rosati, Injectable hyaluronic acid gel for soft tissue augmentation. A clinical and histological study. *Dermatol. Surg.* **24**, 1317–1325 (1998).
11. S. J. Falcone, R. A. Berg, Crosslinked hyaluronic acid dermal fillers: A comparison of rheological properties. *J. Biomed. Mater. Res. A* **87**, 264–271 (2008).
12. M. R. Homicz, D. Watson, Review of injectable materials for soft tissue augmentation. *Facial Plast. Surg.* **20**, 21–29 (2004).
13. J. Elisseeff, K. Anseth, D. Sims, W. McIntosh, M. Randolph, R. Langer, Transdermal photopolymerization for minimally invasive implantation. *Proc. Natl. Acad. Sci. U.S.A.* **96**, 3104–3107 (1999).
14. J. L. Hill-West, S. M. Chowdhury, M. J. Slepian, J. A. Hubbell, Inhibition of thrombosis and intimal thickening by in situ photopolymerization of thin hydrogel barriers. *Proc. Natl. Acad. Sci. U.S.A.* **91**, 5967–5971 (1994).
15. T. B. Fitzpatrick, The validity and practicality of sun-reactive skin types I through VI. *Arch. Dermatol.* **124**, 869–871 (1988).
16. G. R. Cosgrove, J. B. Delashaw, J. A. Grotenhuis, J. M. Tew, H. Van Loveren, R. F. Spetzler, T. Payner, G. Rosseau, M. E. Shaffrey, L. N. Hopkins, R. Byrne, A. Norbash, Safety and efficacy of a novel polyethylene glycol hydrogel sealant for watertight dural repair. *J. Neurosurg.* **106**, 52–58 (2007).
17. J. C. Wain, L. R. Kaiser, D. W. Johnstone, S. C. Yang, C. D. Wright, J. S. Friedberg, R. H. Feins, R. F. Heitmiller, D. J. Mathisen, M. R. Selwyn, Trial of a novel synthetic sealant in preventing air leaks after lung resection. *Ann. Thorac. Surg.* **71**, 1623–1628 (2001).
18. R. Laszig, G. J. Ridder, M. Fradis, Intracochlear insertion of electrodes using hyaluronic acid in cochlear implant surgery. *J. Laryngol. Otol.* **116**, 371–372 (2002).
19. A. Storr-Paulsen, J. C. Nørregaard, G. Farik, J. Tårnhøj, The influence of viscoelastic substances on the corneal endothelial cell population during cataract surgery: A prospective study of cohesive and dispersive viscoelastics. *Acta Ophthalmol. Scand.* **85**, 183–187 (2007).
20. S. L. Matarasso, Understanding and using hyaluronic acid. *Aesthet. Surg. J.* **24**, 361–364 (2004).
21. N. A. Peppas, E. W. Merrill, Poly(vinyl alcohol) hydrogels: Reinforcement of radiation-crosslinked networks by crystallization. *J. Polym. Sci. Polym. Chem. Ed.* **14**, 441–457 (1976).
22. J. Kablik, G. D. Monheit, L. Yu, G. Chang, J. Gershkovich, Comparative physical properties of hyaluronic acid dermal fillers. *Dermatol. Surg.* **35** (Suppl. 1), 302–312 (2009).
23. P. N. Patel, C. K. Smith, C. W. Patrick Jr., Rheological and recovery properties of poly(ethylene glycol) diacrylate hydrogels and human adipose tissue. *J. Biomed. Mater. Res. A* **73A**, 313–319 (2005).
24. S. L. Schor, I. R. Ellis, K. Harada, K. Motegi, A. R. Anderson, M. A. Chaplain, R. P. Keatch, A. M. Schor, A novel 'sandwich' assay for quantifying chemo-regulated cell migration within 3-dimensional matrices: Wound healing cytokines exhibit distinct motogenic activities compared to the transmembrane assay. *Cell Motil. Cytoskeleton* **63**, 287–300 (2006).
25. M. Shah, D. M. Foreman, M. W. Ferguson, Neutralisation of TGF-β1 and TGF-β2 or exogenous addition of TGF-β3 to cutaneous rat wounds reduces scarring. *J. Cell Sci.* **108** (Pt 3), 985–1002 (1995).
26. R. S. Narins, W. P. Coleman III, R. G. Glogau, Recommendations and treatment options for nodules and other filler complications. *Dermatol. Surg.* **35** (Suppl. 2), 1667–1671 (2009).
27. A. T. Hillel, S. Varghese, J. Petsche, M. J. Shamblott, J. H. Elisseeff, Embryonic germ cells are capable of adipogenic differentiation in vitro and in vivo. *Tissue Eng. Part A* **15**, 479–486 (2009).
28. S. Varghese, N. S. Hwang, A. Ferran, A. Hillel, P. Theprungsirikul, A. C. Canver, Z. Zhang, J. Gearhart, J. Elisseeff, Engineering musculoskeletal tissues with human embryonic germ cell derivatives. *Stem Cells* **28**, 765–774 (2010).
29. C. Chung, J. A. Burdick, Influence of three-dimensional hyaluronic acid microenvironments on mesenchymal stem cell chondrogenesis. *Tissue Eng. Part A* **15**, 243–254 (2009).
30. M. Halbleib, T. Skurk, C. de Luca, D. von Heimburg, H. Hauner, Tissue engineering of white adipose tissue using hyaluronic acid-based scaffolds. I: In vitro differentiation of human adipocyte precursor cells on scaffolds. *Biomaterials* **24**, 3125–3132 (2003).
31. B. Bandyopadhyay, J. Fan, S. Guan, Y. Li, M. Chen, D. T. Woodley, W. Li, A "traffic control" role for TGFβ3: Orchestrating dermal and epidermal cell motility during wound healing. *J. Cell Biol.* **172**, 1093–1105 (2006).
32. A. S. Ross, A. K. Bhan, M. Pascual, M. Thiim, A. Benedict Cosimi, R. T. Chung, Pegylated interferon α-2b plus ribavirin in the treatment of post-liver transplant recurrent hepatitis C. *Clin. Transplant.* **18**, 166–173 (2004).
33. D. Mathis, S. E. Shoelson, Immunometabolism: An emerging frontier. *Nat. Rev. Immunol.* **11**, 81 (2011).
34. B. C. Hirsh, W. C. Johnson, Pathology of granulomatous diseases. Foreign body granulomas. *Int. J. Dermatol.* **23**, 531–538 (1984).
35. M. Ghislanzoni, F. Bianchi, M. Barbareschi, E. Alessi, Cutaneous granulomatous reaction to injectable hyaluronic acid gel. *Br. J. Dermatol.* **154**, 755–758 (2006).
36. A. D. Lynn, T. R. Kyriakides, S. J. Bryant, Characterization of the in vitro macrophage response and in vivo host response to poly(ethylene glycol)-based hydrogels. *J. Biomed. Mater. Res. A* **93**, 941–953 (2010).
37. D. S. Raso, W. B. Greene, R. A. Harley, J. C. Maize, Silicone deposition in reconstruction scars of women with silicone breast implants. *J. Am. Acad. Dermatol.* **35**, 32–36 (1996).
38. C. W. Hanke, H. R. Higley, D. M. Jolivette, N. A. Swanson, S. J. Stegman, Abscess formation and local necrosis after treatment with Zyderm or Zyplast collagen implant. *J. Am. Acad. Dermatol.* **25**, 319–326 (1991).
39. N. J. Lowe, C. A. Maxwell, P. Lowe, M. G. Duick, K. Shah, Hyaluronic acid skin fillers: Adverse reactions and skin testing. *J. Am. Acad. Dermatol.* **45**, 930–933 (2001).
40. T. Tagami, Y. Uehara, N. Moriyoshi, T. Ishida, H. Kiwada, Anti-PEG IgM production by siRNA encapsulated in a PEGylated lipid nanocarrier is dependent on the sequence of the siRNA. *J. Control Release* **151**, 149–154 (2011).
41. T. Ishida, X. Wang, T. Shimizu, K. Nawata, H. Kiwada, PEGylated liposomes elicit an anti-PEG IgM response in a T cell-independent manner. *J. Control Release* **122**, 349–355 (2007).

42. **Acknowledgments:** We thank A. Afthinos for his work with cell culture and gene analysis. **Funding:** The research was supported by a grant from Kythera Biopharmaceuticals. **Author contributions:** A.T.H. participated in the technology design, data analysis, and manuscript preparation. Z.N., J.A., and J.J.C. performed most of the animal studies and their respective data analyses. J.M.C. performed the rheological studies. Q.G. optimized implant design and performed light microscopy. S.U. participated in animal studies and manuscript preparation. Z.H. and S.M. performed the animal MRI studies and analysis. R.T., A.T., and B.R. designed and tested the LED. P.W. designed and managed the pilot clinical testing. N.D. participated in technology design. S.L., C.M., and D.S. participated in experimental planning and data analysis. J.M.T. designed immunohistochemical experiments and reviewed histology and immunohistochemistry. J.H.E. was involved in conception of the project, experimental design and analysis, and preparation of the manuscript. **Competing interests:** J.H.E. and A.T.H. are inventors on intellectual property owned by Johns Hopkins University covering light-activated hyaluronic acid biomaterials. J.H.E. is a science advisory board member of Kythera Biopharmaceuticals.

Submitted 25 February 2011
Accepted 8 July 2011
Published 27 July 2011
10.1126/scitranslmed.3002331

Citation: A. T. Hillel, S. Unterman, Z. Nahas, B. Reid, J. M. Coburn, J. Axelman, J. J. Chae, Q. Guo, R. Trow, A. Thomas, Z. Hou, S. Lichtsteiner, D. Sutton, C. Matheson, P. Walker, N. David, S. Mori, J. M. Taube, J. H. Elisseeff, Photoactivated composite biomaterial for soft tissue restoration in rodents and in humans. *Sci. Transl. Med.* **3**, 93ra67 (2011).